Published by IOP Publishing for Sissa Medialab

Received: *November 26, 2025*
Accepted: *December 18, 2025*
Published: *March 10, 2026*

17th Topical Seminar on Innovative Particle and Radiation Detectors
Siena, Italy
15–19 September 2025

HELIX balloon experiment: light cosmic-ray isotopes as probes of Galactic propagation

K. Sakai[a,*] **P. Allison**[b] **A. Bhardwaj**[c] **J.J. Beatty**[b] **L. Beaufore**[b] **D.H. Calderon**[b] **Y. Chen**[d] **S. Coutu**[d] **D. Fuehne**[e] **N. Green**[f] **D. Hanna**[g] **H.B. Jeon**[a,h] **S.B. Klein**[i] **K. McBride**[e,j] **C. McGrath**[c] **S.I. Mognet**[d] **J. Musser**[i] **S. O'Brien**[g] **S. Nutter**[k] **N. Park**[c] **M. Tabata**[l] **G. Tarle**[f] **G. Visser**[i] **and S.P. Wakely**[a,e,j]

[a] *Enrico Fermi Inst., University of Chicago, Chicago, IL 60637, U.S.A.*
[b] *Department of Physics, Center for Cosmology and AstroParticle Physics, Ohio State, Columbus, OH 43210, U.S.A.*
[c] *Department of Physics, Engineering Physics and Astronomy, Queen's University, Kingston, ON K7L 3N6, Canada*
[d] *Department of Physics, Inst. for Gravitation and the Cosmos, Pennsylvania State University, University Park, PA 16802, U.S.A.*
[e] *Department of Physics, University of Chicago, Chicago, IL 60637, U.S.A.*
[f] *Department of Physics, University of Michigan, Ann Arbor, MI 48109, U.S.A.*
[g] *Department of Physics, McGill University, Montréal, QC H3A 2T8, Canada*
[h] *NASA Goddard Space Flight Center, Greenbelt, MD 20771, U.S.A.*
[i] *Department of Physics, Indiana University, Bloomington, ID 47405, U.S.A.*
[j] *Kavli Inst. for Cosmological Physics, University of Chicago, Chicago, IL 60637, U.S.A.*
[k] *Department of Physics, Geology and Engineering Tech, Northern Kentucky University, Highland Heights, KY 41076, U.S.A.*
[l] *Department of Physics, Chiba University, Chiba 263-0022, Japan*

E-mail: kenichisakai@uchicago.edu

Abstract: Beryllium isotopes, particularly ^{10}Be, provide a direct measurement of cosmic-ray lifetimes, enabling strong constraints on their propagation and the size of the Galactic halo. High-precision, mass-resolved measurements above ~2 GeV/n have not been previously achieved. The High Energy Light Isotope eXperiment (HELIX) is a balloon-borne magnetic spectrometer designed to measure the charge, velocity, and rigidity of cosmic rays, allowing isotope separation of beryllium and other light nuclei. The initial engineering flight, conducted from Esrange, Sweden in the boreal spring of 2024, targeted instrument performance up to ~3 GeV/n. Here, we present an overview of the payload, flight operations, and preliminary analysis efforts.

Keywords: Balloon instrumentation; Spectrometers

*Corresponding author.

https://doi.org/10.1088/1748-0221/21/03/C03014

Contents

1 Introduction

Numerous satellite missions [1–3], experiments on the International Space Station (ISS) [4, 5], and high-altitude balloon observations [6–9] have precisely measured the cosmic-ray spectrum. Nevertheless, many fundamental questions remain unresolved, such as the nature of dark matter [10] and the structure of our Galaxy. One promising approach to dark matter searches is the detection of antiparticles. Inspired by the potential observation of antihelium candidates by AMS-02 [11, 12], several new experiments are being conducted or planned [9, 13].

Among the cosmic-ray species expected to provide key insights is beryllium-10 (^{10}Be), although it has rarely been measured due to its experimental difficulties. The challenge arises primarily from the relatively small mass difference between ^{9}Be and ^{10}Be; without exceptionally high mass resolution, the individual mass peaks cannot be resolved. Analyses based on unresolved mass distribution peaks depend on assumptions derived from existing models, effectively constraining the result to follow standard expectations. Consequently, they cannot yield independent or potentially unexpected findings. Existing measurements, including those by ISOMAX [14] and PAMELA [15], have been limited by statistical uncertainty and mass resolution.

The ^{10}Be nuclei observed with high precision by the HELIX experiment [8], which employs a superconducting magnetic spectrometer, have both theoretical and observational significance. Figure 1 shows the HELIX payload at the launch site in an image taken around the time of the initial balloon campaign, which launched on May 28, 2024. Because ^{10}Be is a radioactive isotope with a half-life of 1.39 Myr, it serves as a "clock" for determining the age of cosmic rays. Although several uncertainties remain due to residual atmospheric effects during balloon

Figure 1. A picture of the HELIX payload for its first balloon flight just before launch from Esrange, Sweden. The solar array hangs below the bottom of the white gondola.

2026 JINST 21 C03014

flights, secondary production details from C, N, and O nuclei, and solar modulation, ^{10}Be measurements can place strong constraints on the diffusion coefficient and the size of the Galactic halo, parameters that cannot be fully determined from the boron-to-carbon (B/C) ratio [16] alone.

A precise description of cosmic-ray propagation, as revealed by ^{10}Be measurements, is also essential for interpreting phenomena such as the positron excess [1–6], and thus contributes indirectly to dark matter searches. Beyond constraining transport parameters, high-precision isotope data provide valuable cross-checks on the overall consistency of cosmic-ray models and can help identify tensions that might point to additional physics or unmodeled astrophysical contributions.

2 Instrument capabilities

HELIX is a superconducting magnetic spectrometer optimized for direct isotope identification of light cosmic-ray nuclei. Its design integrates multiple complementary detector systems to measure rigidity, velocity, and charge with unprecedented precision.

2.1 Measurement principle

As shown in figure 2, cosmic-ray particles are tracked through an average 1.0 T magnetic field to determine their rigidity ($R = pc/Ze$) by the drift chamber tracker (DCT). Charge (Z) is measured by a time-of-flight (TOF) system, while the particle velocity (β) is determined from the TOF at low energies and from the ring-imaging Cherenkov (RICH) detector at higher energies. Combining these measurements yields the particle mass:

$$mc^2 = \frac{RZe}{\gamma\beta}, \qquad \left(\frac{\delta m}{m}\right)^2 = \left(\frac{\delta R}{R}\right)^2 + \gamma^4\left(\frac{\delta\beta}{\beta}\right)^2$$

To separate beryllium isotopes, HELIX is designed to achieve better than 2.5% resolution in both rigidity ($\delta R/R$) and velocity ($\gamma^2\delta\beta/\beta$). This allows event-by-event identification of isotopes, avoiding reliance on model-dependent spectral fitting.

2.2 Staged development

HELIX employs a staged approach to balance technical readiness with science objectives, as illustrated in figure 3:

- **Stage 1 (Engineering Flight, 2024):** Demonstrated and flown configuration including a 1 T superconducting magnet, DCT, TOF, hodoscope, and RICH. Operated successfully up to $\sim$ 3 GeV/n.
- **Stage 2 (Science Flight):** Adds one or two silicon tracking layers to extend the maximum detectable rigidity (MDR) and enhance high-energy isotope identification.

2.3 Subsystem descriptions

Figure 4 summarizes the primary detector components developed and integrated for the HELIX Stage 1.

Superconducting Magnet. HELIX employs the HEAT superconducting magnet [6].

- *Cryogenics:* A liquid-helium cryostat maintains the magnet at 4 K.

2026 JINST 21 C03014

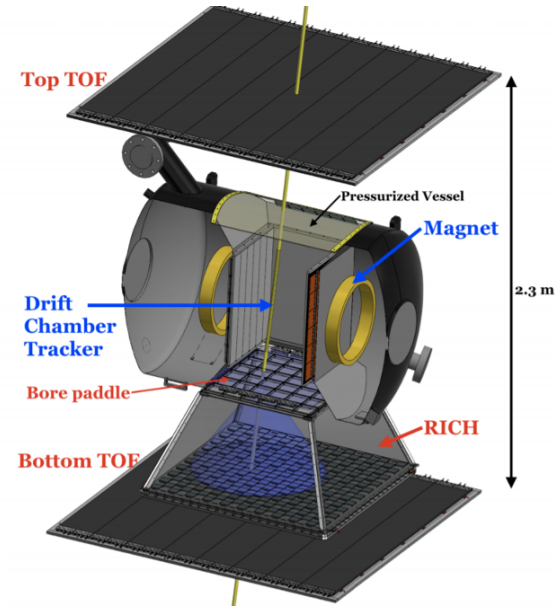

Figure 2. Rendering of the HELIX detector showing the main subsystems. Cutouts of the superconducting magnet coils and the tracker are visible. The RICH system is shown with the aerogel array and the SiPM focal-plane readout.

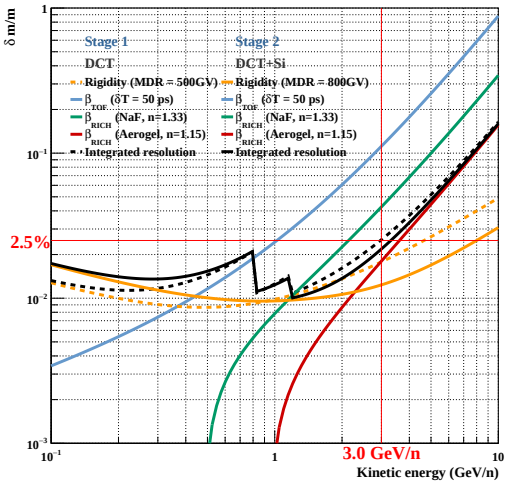

Figure 3. Relative mass resolution ($\delta m/m$) vs. kinetic energy. HELIX is designed to achieve a mass resolution of about 2.5%, sufficient to resolve ^{9}Be and ^{10}Be mass peaks and thus unlock key physics of cosmic-ray propagation.

- *Field Strength:* Provides an average magnetic field of approximately 1 Tesla within the DCT tracking volume, as shown in figure 5.
- *Geometry:* Features an open bore with negligible material above and below, minimizing grammage for incoming and outgoing particles.

Drift Chamber Tracker (DCT). The DCT measures particle rigidity by reconstructing the trajectory curvature within the magnetic field.

- *Principle:* Charged particles ionize a CO_2-Ar gas mixture (90:10) at 1 atm. The resulting electrons drift to sense wires under a 0.8 kV/cm field.
- *Configuration:* Three drift-cell planes, each containing 72 sense wires, along the vertical direction in the HELIX coordinate system.
- *Measurement:* In the bending plane, drift distance is derived from ionization timing using an 80 MHz readout; in the non-bending plane, position is determined along the sense wire by comparing charges measured at the ends.

Time-of-Flight (TOF) System. The TOF measures both particle velocity and charge.

- *Principle:* Scintillator paddles emit light as particles traverse them; the light is read out at both ends using silicon photomultipliers (SiPMs).
- *TDC:* The system uses a coarse 25-ns TDC measurement combined with a ramp-shaping technique, enabling the ADC to extract fine timing information and enhance the effective timing resolution.

2026 JINST 21 C03014

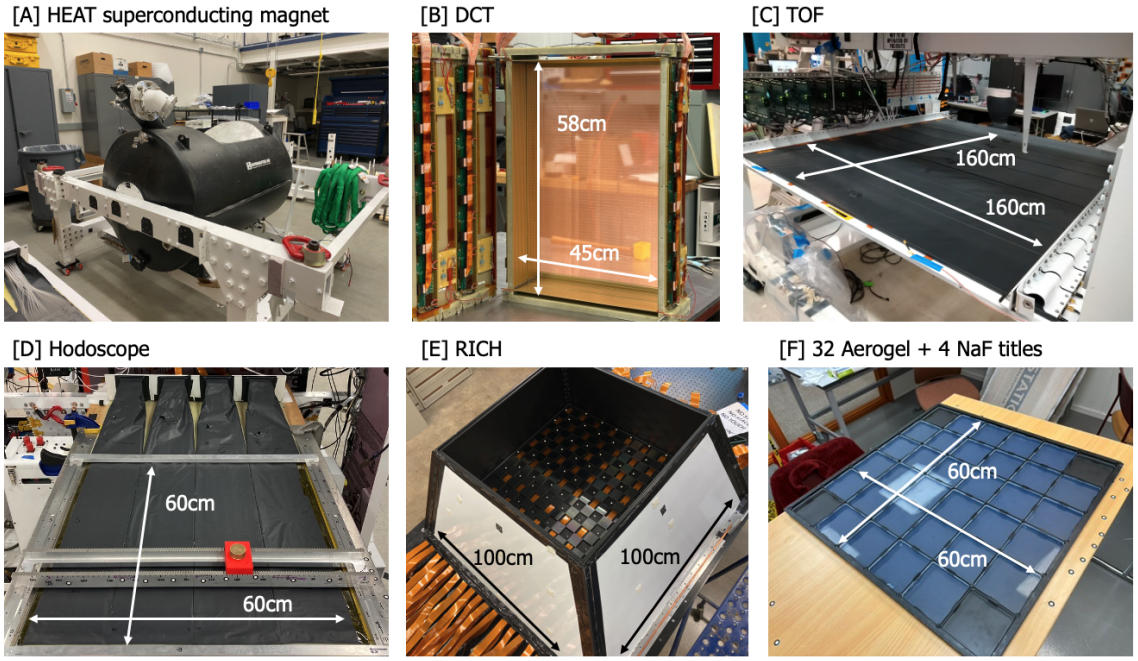

Figure 4. Photographs of major HELIX detector subsystems: (A) HEAT superconducting magnet; (B) a single plane of 72 sense wires before assembly with the rest of the DCT components; (C) bottom TOF scintillator paddles; (D) ribbon-fiber hodoscope; (E) RICH detector with SiPM focal plane readout; and (F) radiator assemblies (32 aerogel and 4 NaF tiles).

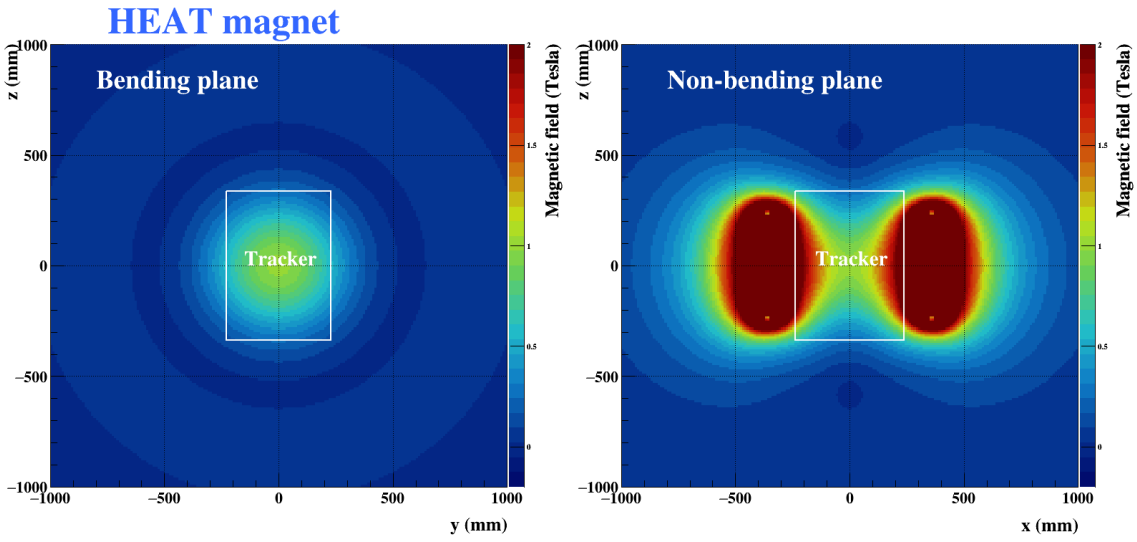

Figure 5. Mapped magnetic field strength (Tesla) in the bending plane (left) and non-bending plane (right).

- *Geometry:* Three planes-top, bottom, and an aperture-defining layer located below the DCT. The total vertical separation from top to bottom is approximately 2.3 m.
- *Performance:* Provides β measurement up to $\sim$ 1 GeV/n (critical for the RICH transition) and charge identification from light amplitude.

2026 JINST 21 C03014

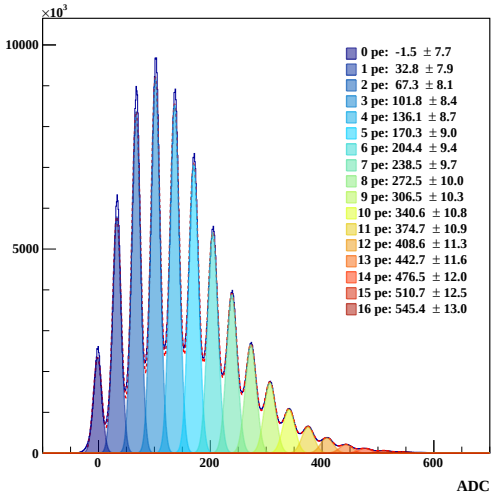

Figure 6. Summed ADC spectrum from all 200 SiPM arrays (12,800 channels) during laser calibration. The photoelectron peaks are clearly separated with a spacing of about 35 ADC counts, demonstrating excellent gain uniformity across the focal plane.

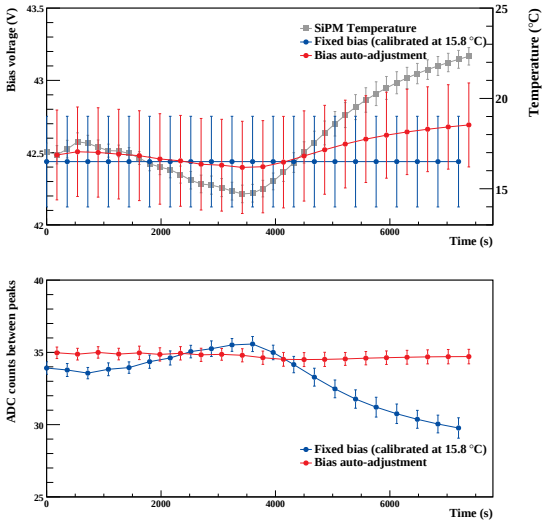

Figure 7. Top: SiPM temperature and applied bias vs. time; bottom: ADC peak spacing. Under fixed bias (blue), temperature variations change the gain. With automatic bias adjustment (red), the peak spacing remains stable.

Hodoscope. The hodoscope refines tracking in the non-bending plane and improves tracking determination for RICH β reconstruction.

- *Design:* 600 square scintillating fibers, each 1 mm thick.
- *Readout:* Fibers coupled to SiPMs, with 150 fibers multiplexed to 64 SiPMs (2–3 fibers per channel).
- *Performance:* Track matching efficiency of approximately 90%, with ongoing optimization to enhance hit selection accuracy.

Ring Imaging Cherenkov (RICH) Detector. HELIX deploys the first aerogel-SiPM proximity-focused RICH ever flown on a balloon experiment.

- *Principle:* Relativistic particles (kinetic energy > 1 GeV/n) emit Cherenkov radiation in aerogel.
- *Radiator:* High-refractive-index ($n \approx 1.15$) transparent aerogel, beam-calibrated to precision of $O(10^{-4})$ [17, 18].
- *Photon Detection:* A 1 m^2 SiPM focal plane (half-populated in Stage 1) comprising 200 arrays, each made of 64 individual SiPMs with 6×6 mm^2 pixels and 75 µm microcells, totaling 12,800 pixels. Figure 6 shows the summed ADC spectrum during laser calibration, with clearly separated peaks demonstrating excellent uniformity across the focal plane.
- *Bias Auto-Adjustment:* SiPM gain varies with temperature. Since signals below 0.5 PE are masked online and cannot be recalibrated in offline analysis, an automatic bias-control algorithm adjusts the bias to keep the ADC peak spacing at 35 counts, as shown in figure 7.

Together, these subsystems provide a unified, redundant measurement of rigidity, velocity, and charge, achieving the resolution required to resolve isotopic mass peaks. The demonstrated Stage 1

2026 JINST 21 C03014

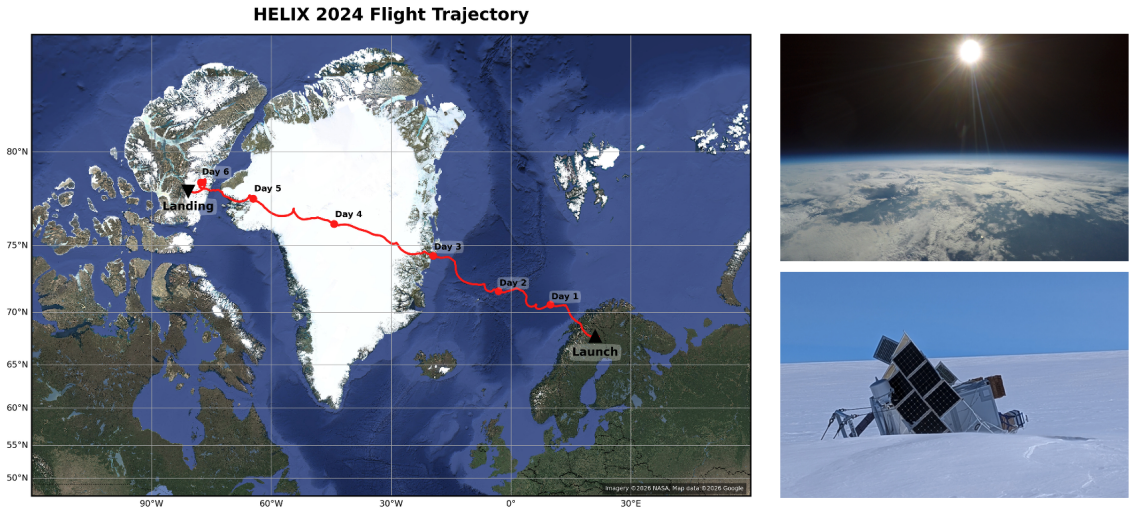

Figure 8. Merged figure showing the Stage 1 engineering flight: left, trajectory map; right upper, view from onboard instruments; right lower, payload recovery after landing on Ellesmere Island, Canada. Imagery ©2026 NASA, Map data ©2026 Google [19].

performance validates this integrated design and establishes the foundation for the forthcoming science flight.

3 Engineering flight details (Stage 1)

The first HELIX engineering flight was successfully completed during NASA's Spring 2024 Arctic campaign. The mission was launched from the Esrange Space Center, Kiruna, Sweden, on May 28, 2024, and terminated after 6.3 days, covering a northwestern trajectory from the launch site. Despite a challenging landing location, the payload was safely recovered, enabling subsequent data analysis. Over 120 million triggers were recorded during the flight, validating the functionality of all major subsystems.

3.1 Flight summary

Table 1 summarizes the key parameters of the Stage 1 engineering flight.

Table 1. Summary of the HELIX Stage 1 engineering flight. The trajectory map is shown in figure 8.

Parameter	Value
Launch date	May 28, 2024
Flight duration	6.3 days
Flight path	North and west from Kiruna, Sweden (68° latitude)
Landing site	Ellesmere Island, Canada (78° latitude)
Data collected	>120 million triggers

The successful engineering flight provided a critical test of the HELIX payload, confirming the functionality of all major subsystems including DCT, TOF system, hodoscope, RICH detector, and superconducting magnet, and establishing a solid foundation for the subsequent anticipated Antarctic science flights.

2026 JINST 21 C03014

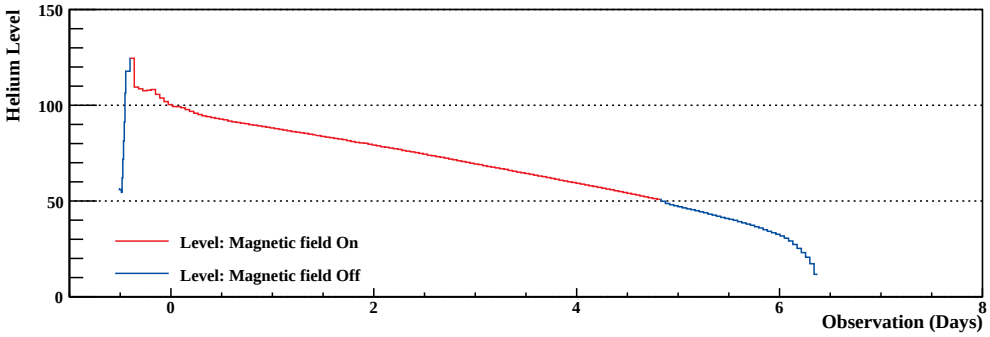

Figure 9. The LHe level vs. observation days during the Stage 1 engineering flight.

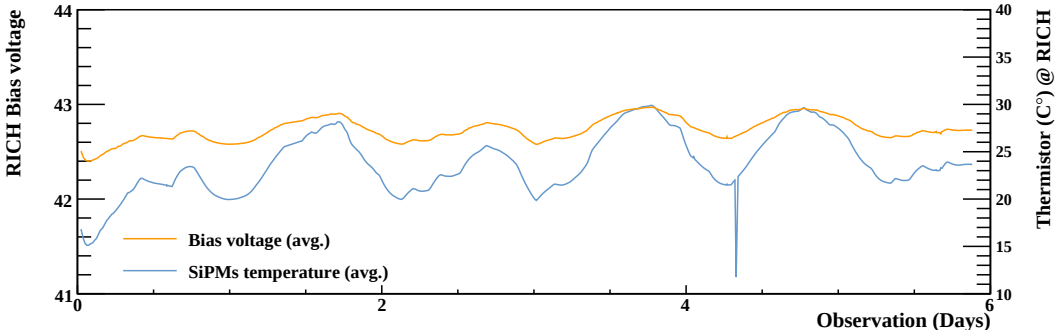

Figure 10. RICH SiPM temperature and bias voltage vs. observation days during the Stage 1 engineering flight.

3.2 Superconducting magnet operation

The liquid helium (LHe) was transferred into the reservoir on the scheduled flight day, and the magnet was energized just prior to launch. Although the magnet was expected to maintain its field for more than six days, the B field was intentionally turned off just under five days after launch to accumulate calibration data without a magnetic field, as shown in figure 9.

Data acquired while the magnet was energized will be used for scientific analysis, while the data collected without a magnetic field serve primarily for detector calibration and performance studies. Ground-based muon data were also useful during the preparation phase, providing straight tracks for initial detector checks.

3.3 RICH cooling system limitation

While nearly all instruments operated under ideal conditions, the RICH cooling system exhibited a limitation during a portion of the flight, causing the SiPM temperature to rise to around 30°C, higher than the originally expected operating temperature near 0°C (figure 10). Despite this, the automatic bias-adjustment system functioned as designed, maintaining stable gain across the focal plane. The elevated temperatures led to increased noise in the SiPM signals; however, RICH rings were successfully observed by applying a timing-based cut in the analysis. As an engineering flight, this issue provided valuable insight into instrument behavior under flight conditions and represents an identified challenge to be addressed in future Antarctic science flights. Further discussion of this performance and mitigation strategy will be provided in the next section.

2026 JINST 21 C03014

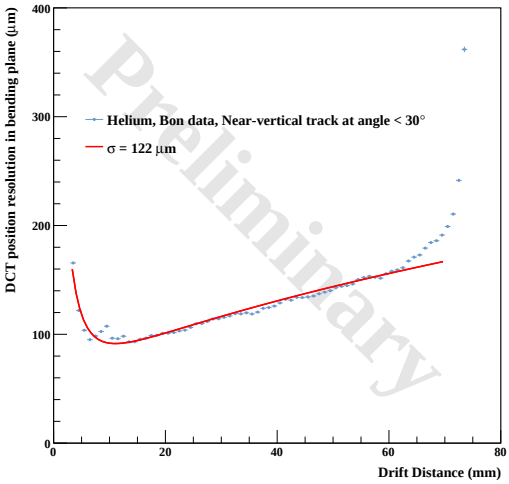

Figure 11. Position resolution in the bending plane obtained from helium events in flight with magnet ON. The drift chamber achieves an average resolution of $\sim$ 120 µm. The calibration relies on Garfield++ simulations that reproduce the isochrones.

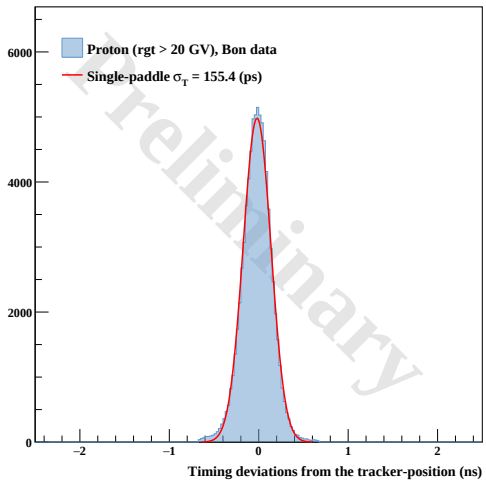

Figure 12. Single-paddle timing resolution of the middle section of the top TOF layer for protons, measured as $(t_0 + t_1)/2$ (in practice inferred from the corrected $(t_0 - t_1)/2$ residuals). The single-paddle resolution is $\sim$ 155.4 ps; the full top-bottom system resolution is expected to be $\sim \sqrt{2}$ larger.

4 Demonstration of instrument performance achieved to date

Analysis of the Stage 1 engineering flight data has already demonstrated key aspects of HELIX detector performance.

Figures 11 and 12 summarize the current position and timing resolutions of the system, based on Stage 1 data and ongoing calibration efforts. In the bending plane, the drift chamber provides an average position resolution of $\sim$ 120 µm for helium events in flight data acquired while the magnet field was on (B-on data), in good agreement with Garfield++ simulations of the isochrones under a uniform 1 T magnetic field. The time-of-flight performance is characterized by the single-paddle timing resolution of the top TOF layer for protons, which is $\sim$ 155.4 ps; combining measurements from the top and bottom layers, the full TOF system resolution is expected to degrade by a factor of $\sqrt{2}$, yielding $\sim$ 220 ps for $Z = 1$ particles, close to the design value. Ongoing calibration and reconstruction improvements are expected to further approach the design goals.

Figures 13 and 14 summarize early results from the particle identification and RICH analyses. Figure 13 shows the correlation between the specific ionization loss (dE/dx) and particle velocity ($\beta\gamma$). Although the tracking calibration is not yet sufficient to use rigidity as the horizontal axis, the current analysis employs the TOF-based $\beta\gamma$ instead. Even with this preliminary method, distinct particle bands are visible, and beryllium candidates are clearly separated, demonstrating that the payload successfully recorded high-quality data for the primary science target.

Figure 14 shows an example event display for a beryllium candidate, where a clear Cherenkov ring is visible. The ring clarity was achieved by applying a timing-based noise suppression cut, which efficiently removed spurious SiPM pulses caused by the elevated temperature observed during flight.

2026 JINST 21 C03014

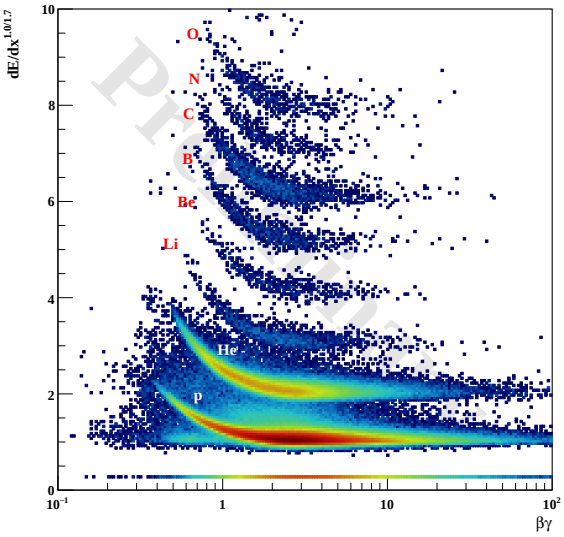

Figure 13. dE/dx vs. $\beta\gamma$ from the Stage 1 engineering flight, obtained using TOF data. Despite the absence of full tracking calibration, clear particle bands are visible, including a distinct Be band.

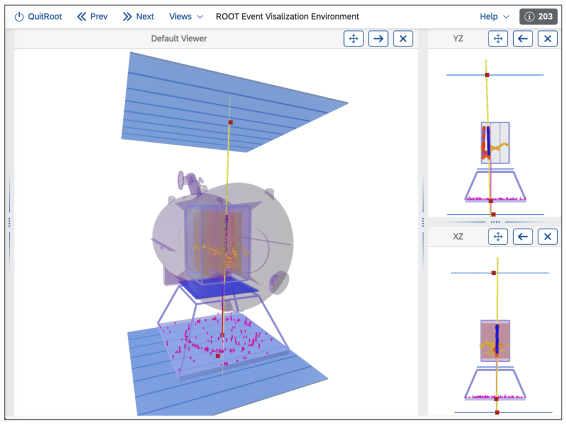

Figure 14. Event display of a beryllium candidate from the Stage 1 engineering flight. A clear Cherenkov ring is visible after applying the timing-based cut to suppress SiPM noise.

This confirms that the RICH detector operated as designed under flight conditions, and that useful data could be extracted despite the temporary cooling system limitation.

These results confirm that the major detector subsystems performed as expected and that the engineering flight successfully met its objective of validating detector functionality and data quality. Ongoing work focuses on refining the tracking calibration and reconstruction algorithms, which will enable the use of dE/dx vs. rigidity plots for comprehensive particle identification in future Antarctic science flights.

5 Conclusions

The first engineering flight of HELIX Stage 1 was successfully completed in 2024, and the payload was safely recovered. All detector systems remained operational and are undergoing further testing and refurbishment. Preliminary analysis indicates that the subsystems performed reliably and that data of sufficient quality were collected for beryllium isotope identification. Observed Cherenkov rings in the RICH system confirm its functionality during flight conditions. These results provide a solid foundation for refining the instrument and preparing for subsequent Antarctic science flights, including upgrades to the gondola structure.

Acknowledgments

This work is supported in the US by grant 80NSSC20K1840 from the National Aeronautics and Space Administration (NASA), and in Canada by grants from the Natural Sciences and Engineering Research Council (NSERC) and the Canadian Space Agency's FAST program. We also gratefully acknowledge the Columbia Scientific Balloon Facility (CSBF) and the Swedish Space Corporation (SSC) for their balloon operations support at Esrange Space Center.

2026 JINST 21 C03014

References

[1] Fermi-LAT collaboration, *Cosmic-ray electron-positron spectrum from 7 GeV to 2 TeV with the Fermi Large Area Telescope*, *Phys. Rev. D* **95** (2017) 082007 [arXiv:1704.07195].

[2] PAMELA collaboration, *An anomalous positron abundance in cosmic rays with energies 1.5–100 GeV*, *Nature* **458** (2009) 607 [arXiv:0810.4995].

[3] DAMPE collaboration, *Direct detection of a break in the teraelectronvolt cosmic-ray spectrum of electrons and positrons*, *Nature* **552** (2017) 63 [arXiv:1711.10981].

[4] AMS collaboration, *High Statistics Measurement of the Positron Fraction in Primary Cosmic Rays of 0.5–500 GeV with the Alpha Magnetic Spectrometer on the International Space Station*, *Phys. Rev. Lett.* **113** (2014) 121101.

[5] CALET collaboration, *Direct Measurement of the Spectral Structure of Cosmic-Ray Electrons+Positrons in the TeV Region with CALET on the International Space Station*, *Phys. Rev. Lett.* **131** (2023) 191001 [arXiv:2311.05916].

[6] J.J. Beatty et al., *New measurement of the cosmic-ray positron fraction from 5 to 15-GeV*, *Phys. Rev. Lett.* **93** (2004) 241102 [astro-ph/0412230].

[7] K. Abe et al., *Measurements of cosmic-ray proton and helium spectra from the BESS-Polar long-duration balloon flights over Antarctica*, *Astrophys. J.* **822** (2016) 65 [arXiv:1506.01267].

[8] HELIX collaboration, *The High Energy Light Isotope eXperiment program of direct cosmic-ray studies*, 2024 *JINST* **19** C01025 [arXiv:2312.06796].

[9] GAPS collaboration, *Antideuteron Sensitivity for the GAPS Experiment*, *Astropart. Phys.* **74** (2016) 6 [arXiv:1506.02513].

[10] R. Kappl and M.W. Winkler, *Dark Matter after BESS-Polar II*, *Phys. Rev. D* **85** (2012) 123522 [arXiv:1110.4376].

[11] K. Abe et al., *Search for Antihelium with the BESS-Polar Spectrometer*, *Phys. Rev. Lett.* **108** (2012) 131301 [arXiv:1201.2967].

[12] A. Kounine, *AMS experiment on the international space station, next generation of astroparticle experiments in space*, in the proceedings of the *1st Workshop on the Next Generation of AstroParticle Experiments in Space (NextGAPES-2019)*, Moscow, Russia, 21–22 June 2019.

[13] T. Aramaki, P. Hansson Adrian, G. Karagiorgi and H. Odaka, *Dual MeV Gamma-Ray and Dark Matter Observatory — GRAMS Project*, *Astropart. Phys.* **114** (2020) 107 [arXiv:1901.03430].

[14] T. Hams et al., *Measurement of the abundance of radioactive Be-10 and other light isotopes in cosmic radiation up to 2-GeV/nucleon with the balloon-borne instrument ISOMAX*, *Astrophys. J.* **611** (2004) 892.

[15] PAMELA collaboration, *Lithium and Beryllium Isotopes with the PAMELA Experiment*, *Astrophys. J.* **862** (2018) 141 [arXiv:1806.10948].

[16] AMS collaboration, *Precision Measurement of the Boron to Carbon Flux Ratio in Cosmic Rays from 1.9 GV to 2.6 TV with the Alpha Magnetic Spectrometer on the International Space Station*, *Phys. Rev. Lett.* **117** (2016) 231102.

[17] M. Tabata et al., *Developing a silica aerogel radiator for the HELIX ring-imaging Cherenkov system*, *Nucl. Instrum. Meth. A* **952** (2020) 161879 [arXiv:1901.06663].

[18] P. Allison et al., *Electron-beam calibration of aerogel tiles for the HELIX RICH detector*, *Nucl. Instrum. Meth. A* **1055** (2023) 168549 [arXiv:2307.09689].

[19] Google, *Google Maps*, https://www.google.com/maps [Accessed: 2026-01-21].

2026 JINST 21 C03014